Sensors & Actuators: A. Physical 339 (2022) 113509

Contents lists available at ScienceDirect

Sensors and Actuators: A. Physical

journal homepage: www.journals.elsevier.com/sensors-and-actuators-a-physical

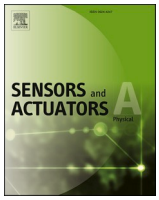

Wind speed measurement with a low-cost polymer optical fiber anemometer based on Fresnel reflection

Mehmet Güçyetmez, Serkan Keser, Şekip Esat Hayber *

Department of Electrical-Electronic Engineering, Kırşehir Ahi Evran University, Kırşehir 40100, Turkey

ARTICLE INFO

Keywords:
Fiber anemometer
Polymer optical fiber
Fresnel reflection

ABSTRACT

This study designed and experimentally verified a simple and low-cost anemometer based on Fresnel reflection using Polymer Optical Fiber (POF). The system was developed especially for wind speed measurement in harsh environmental conditions such as high electromagnetic interference. System verification was performed using a controlled wind source and a high-standard anemometer. In measurements made under normal temperature conditions, the dynamic range of the anemometer is between 3 m/s and 15 m/s. Experiments were carried out with two propellers of different diameters to evaluate the propeller diameter effect. According to the results obtained from the wind speed measurement experiments, it was observed that the mean error value for all measurements was 0.16, and the mean percentage relative error value was 1.85%.

1. Introduction

Wind energy is an essential type of energy among renewable energy sources, so it has grown by 30% annually in the last ten years and has shown a significant development [1]. Wind power generation's efficiency is affected mainly by wind speed, air density, air pressure, ambient temperature, wind speed distribution, and turbulence density parameters [2]. Since the power to be obtained from the wind turbine is proportional to the cube of the wind speed [3], in most cases, whether the wind turbine will be installed or where it will be installed depends on the wind speed [4].

Anemometers have measured wind speed differently since they were first developed by the Italian mathematician Leone Battista Alberti [5]. They are crucial devices in terms of increasing the energy efficiency obtained from the wind, thus reducing the energy costs, and incorporating new wind power plant locations into electrical energy generation, thanks to the accurate determination of the wind speed [6]. Another issue that has made anemometers more important in recent years is the spread of small wind turbines and their inclusion in micro and smart grids within the scope of microgeneration [7]. For these reasons, the need for anemometers with low-cost and simple measurement systems has also increased. In addition, the more widespread use of anemometers will make small-scale wind turbines more common [8].

Anemometers can be produced mechanically [9], hot wire [10], ultrasonic [11], lidar [12], fiber optic [13] according to sensing principles. In addition to classical mechanical anemometers, which can be of the cup [14,15], propeller [16], and vane type [17,18], studies are also carried out on airflow detection that use a pitot tube to increase wind density [19]. However, classical mechanical anemometers have the disadvantage of being affected by electrical environments [20,21]. While exposure to electromagnetic interference limits ultrasonic anemometers [22], deterioration in calibration due to ambient temperature and limited operating temperature range [23] are factors that negatively affect the widespread use of hot-wire anemometers.

Fiber optic sensing is another method used to detect wind and airflow. Although the detection of wind speed by fiber optic methods dates back to the 1980s [24], studies on fiber optic anemometers have intensified since 2017 [25–34] due to the acceleration of fiber optic products and the absence of disadvantages in other types of anemometers. The basic principle of fiber optic sensors is based on observing changes in the optical signal traveling along the fiber. An optical field consists of four essential parameters: intensity, polarization, phase, and frequency (wavelength). This effect can be determined by perceiving these parameters' changes with the external effect. Accurately measuring and evaluating changes in parameters is very important for optical sensor reliability. In optical research, phase or frequency detection is called the interferometric technique. Although the sensitivity and resolution of interferometric sensors are better than intensity and polarization-based sensors for some applications, they are more complex than most sensor structures. When we look at the studies made

* Corresponding author.
E-mail addresses: mgucyetmez@ahievran.edu.tr (M. Güçyetmez), skeser@ahievran.edu.tr (S. Keser), sehayber@ahievran.edu.tr (Ş.E. Hayber).

https://doi.org/10.1016/j.sna.2022.113509
Received 13 January 2022; Received in revised form 12 February 2022; Accepted 13 March 2022
Available online 15 March 2022

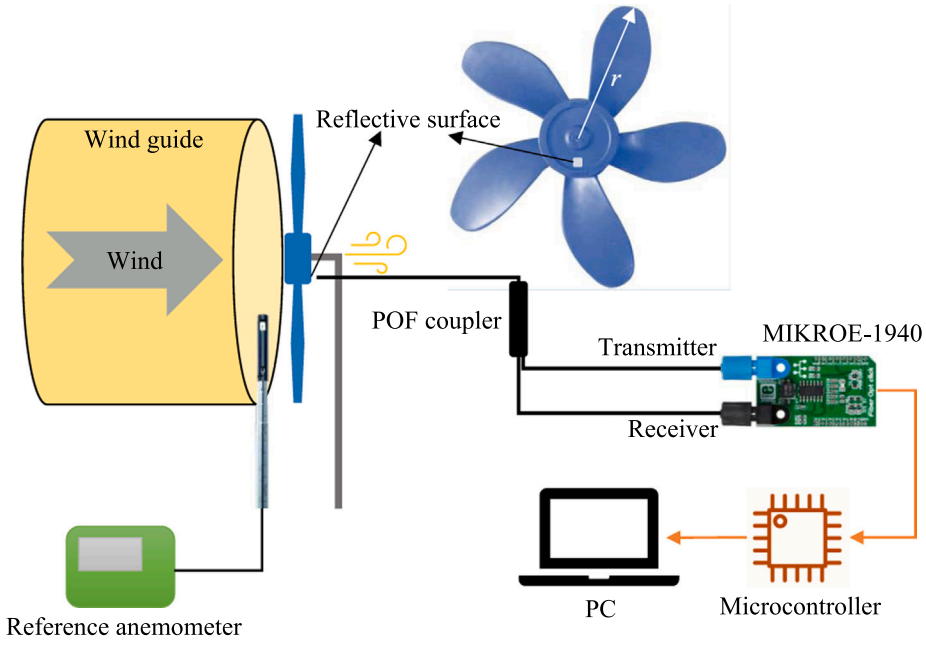

Fig. 1. Schematic representation of the proposed FO-WSMS.

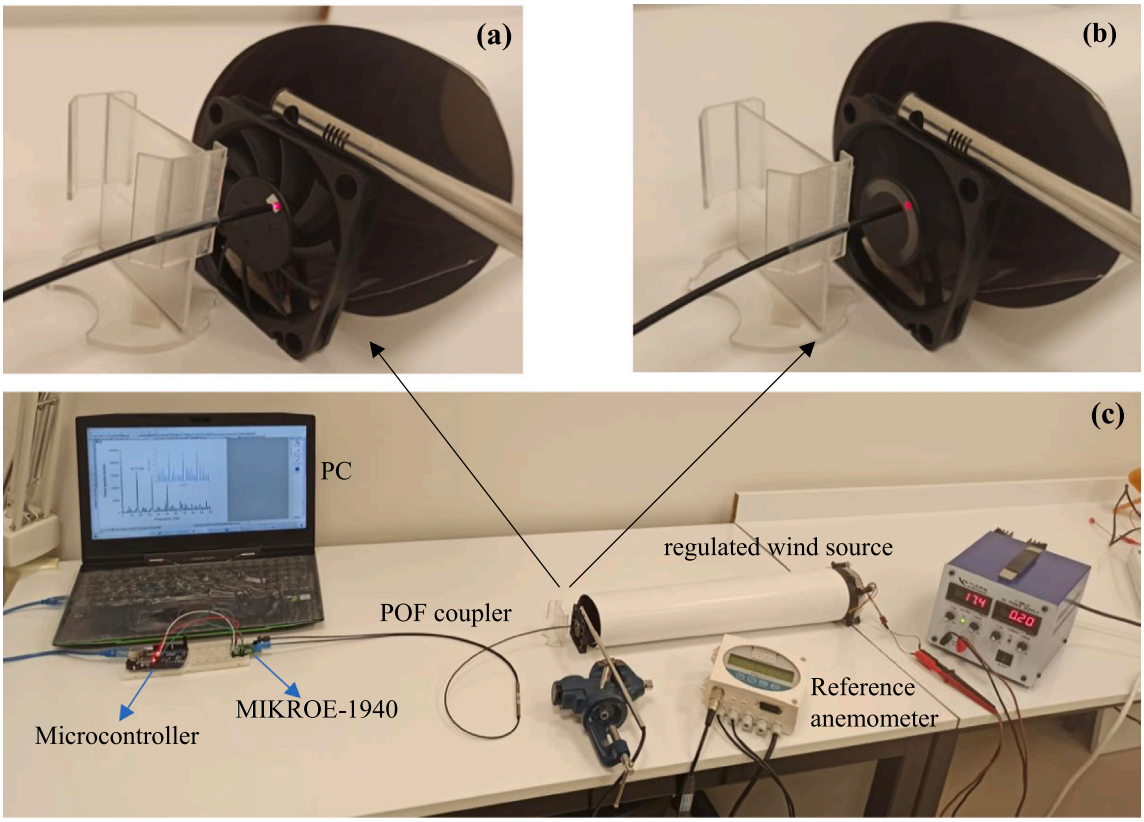

Fig. 2. Fiber sensing tip and reference anemometer (a) no wind, (b) with wind, and (c) the FO-WSMS.

for anemometer in the literature, we see that almost all constitute these Fiber Bragg Grating (FBG)-based systems. Although the FBG technique is one of the widely used techniques in single or multimode fibers for wind speed determination by fiber optic method [25–39], it is a significant disadvantage that it has expensive peripherals such as a broadband light source and optic spectrum analyzer. In addition, such peripherals create a distinct disadvantage for on-site measurement applications. Despite portable, low-cost, and high-performance FBG-based sensor applications available in the literature, they have not yet been used in wind speed measurement studies [40].

There are a few non-FBG-based studies in the literature. Liu et al. report a new fiber-optic anemometer based on a Fabry-Pérot interferometer formed by a thin silicon film adhered to the end face of a single-mode fiber [41]. Although FBG was not used in this study, there are

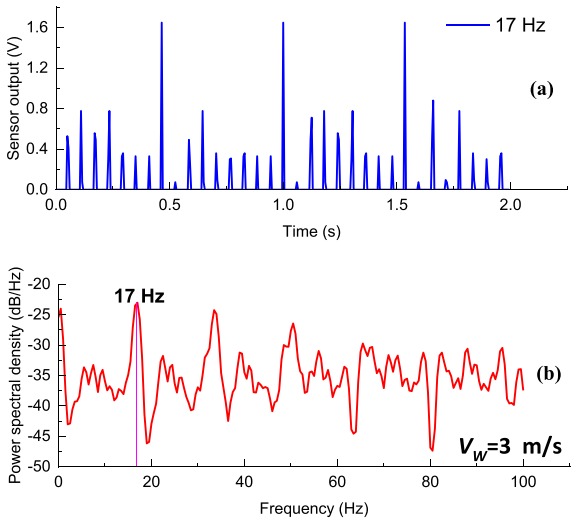

Fig. 3. (a) Time-amplitude, (b) Welch PSD of the signal at a wind speed of 3 m/s.

expensive and complex peripherals. Costa et al. were designed a flow sensor and an anemometer with an optical fiber single mode-multimode-single mode multimodal interference reflective bend structure covered with the gold film [42]. Although Polymer Optical Fibers (POFs) have disadvantages over glass optical fibers in long-range data transmission, POFs offer some advantages in sensor applications based on short-range intensity modulation. POF sensors are applied in different areas like robotics [43], flexible sensor [44], biochemical [45, 46], refractive index [47], oil aging in power transformers [48]. It can be said that these advantages are having more uncomplicated and low-cost components, allowing to operate in the visible spectrum, allowing for greater flexibility and bending, and ease of connection [49]. The number of fiber optic anemometers made with POFs is almost non-existent in the literature. In one of these studies, the POF-based sensor was combined with a wind generator to determine the wind speed [50]. In the study, a Wind Speed Measurement (WSM) was carried out based on the rotation speed of the shaft connected to the wind propeller, so this measurement setup cannot be used to measure an external wind speed [50]. A recent study developed a WSM system based on an intensity-modulated fiber optic curvature sensor [51]. The rotation speed of the propeller used in the system, which has a measuring range of 3–15 m/s, causes tension in the curvature sensor, and the tension is indirectly associated with the wind speed. However, in the related study, the wind speed is measured with losses due to the many mechanical mechanisms.

This study has developed a Fiber Optic-Based Wind Speed Measurement System (FO-WSMS). The wind speed can be determined by directly measuring the rotation speed of a rotating propeller depending on the wind speed. An Opto-mechanic mechanism based on Fresnel reflection was established by increasing the reflectivity of a single point of the propeller. A bidirectional low-cost 1 × 2 POF coupler with a Poly (Methyl Methacrylate) (PMMA) fiber core is used, which allows the optical transceiver to operate on a single line. A micro-card, which is located on the transceiver pair operating at a wavelength of 650 nm, was used compactly. The micro-card is connected to a simple microcontroller circuit. The Power Spectral Density (PSD) was found by applying the Welch method to the signals obtained according to each different wind speed. Thus, the fundamental frequencies indicated by the PSD values were obtained. Wind speeds were determined and compared with the reference anemometer according to these obtained frequencies. As a result of repeated measurements, the mean and percentage relative errors were determined as 0.16% and 1.85%, respectively.

2. Materials and methods

2.1. Design and manufacture of the sensing system

The schematic representation of the FO-WSMS is given in Fig. 1. The measurement system consists of a wind guide that is made of a plastic material with a length of 45 cm and a diameter of 10 cm, a free rotating propeller with a single point reflective surface, a 1 × 2 POF coupler, a fiber opt click card with transceiver inputs, a microcontroller, a PC, and a reference anemometer. The wind guide located at the output of the controlled wind source is approximately the propeller's diameter. The propeller is made of plastic, has a diameter of 5.5 cm, and has an aluminum reflective surface measuring 3 mm × 3 mm, as shown in Fig. 2 (a). The coupler is operationally wavelength-independent and is limited only by the physical properties of the PMMA fiber core. The fiber with a core/cladding diameter of 980/1000 μm in the coupler has a minimum attenuation value at a wavelength of 650 nm. A microe-1940 fiber opt click card features IF-D91 fiber-optic photodiode, IF-E97 fiber-optic LED as well as two operational amplifiers. An Arduino Uno microcontroller was used based on an ATmega328P with a software of Arduino IDE 1.8.19. A Kimo CTV 200-BO Air Velocity/Air Flow Transmitter 24VAC/DC, whose pre-measurement calibrations were made in accordance with the standards, was used.

The proposed FO-WSMS is shown in Fig. 2. Experimental operation under normal conditions (ambient temperature 23 ℃, 1 atmospheric pressure, and humidity 60%). First, the propeller is rotated because of the controlled wind passing through the guide and hitting the propeller (Fig. 2(b)). As shown in Fig. 2(a), the desired wind speed value is adjusted and fixed with the help of the reference anemometer placed in the same position as the propeller. The sensing tip of the POF coupler is aligned and fixed to the reflective surface. Thus, it is ensured that the light rays reflected from the surface can be collected. Light rays are sent from the transmitter on the fiber optic card. The rays coming to the sensing tip via the coupler come out from the tip. Then, the rays that coincide with the reflective surface are reflected from the surface and enter back to the sensing tip. Since the used coupler has a 50:50 split ratio, approximately 50% of the light rays reach the receiver of the fiber optic card. The received light is processed on the fiber optic card and transferred to the microcontroller unit from the RX pin as an analog signal. The microcontroller unit converts this analog signal into a digital signal by sampling it in a suitable sampling period and then sends it to the computer via the serial port.

2.2. Obtaining the PSD of the signals and wind speed

The periodogram method is a fast Fourier transform method based on a non-parametric approach and is one of the classical spectral estimation methods. The PSD equation is given in Eq. (1).

$$P_{xx}(f) = \frac{1}{N}\left|\sum_{n=0}^{N-1} x(n)e^{-j2\pi fn}\right|^2 = \frac{1}{N}|X(f)|^2 \quad (1)$$

Where N is the number of samples of the discrete-time signal x(n), and X (f) is the Fourier transform of $x(n)$. The Welch method was used to calculate the PSD due to the noise in the signals obtained in the time domain. Welch's method can reduce frequency resolution to reduce noise in the estimated power spectrum. Thus, a noiseless modified PSD is obtained according to the Bartlett power spectral method. In order to obtain the modified structure of the periodogram with the Welch method, the signals are first segmented. Then, applying a window to each segment's modified periodogram is found. Segments are typically multiplied by a window function such as a Hamming window. Then, an average periodogram of these obtained periodograms is found. Segments are overlapped while performing the operations mentioned above. The i_{th} modified periodogram is given by Eq. (2) [52].

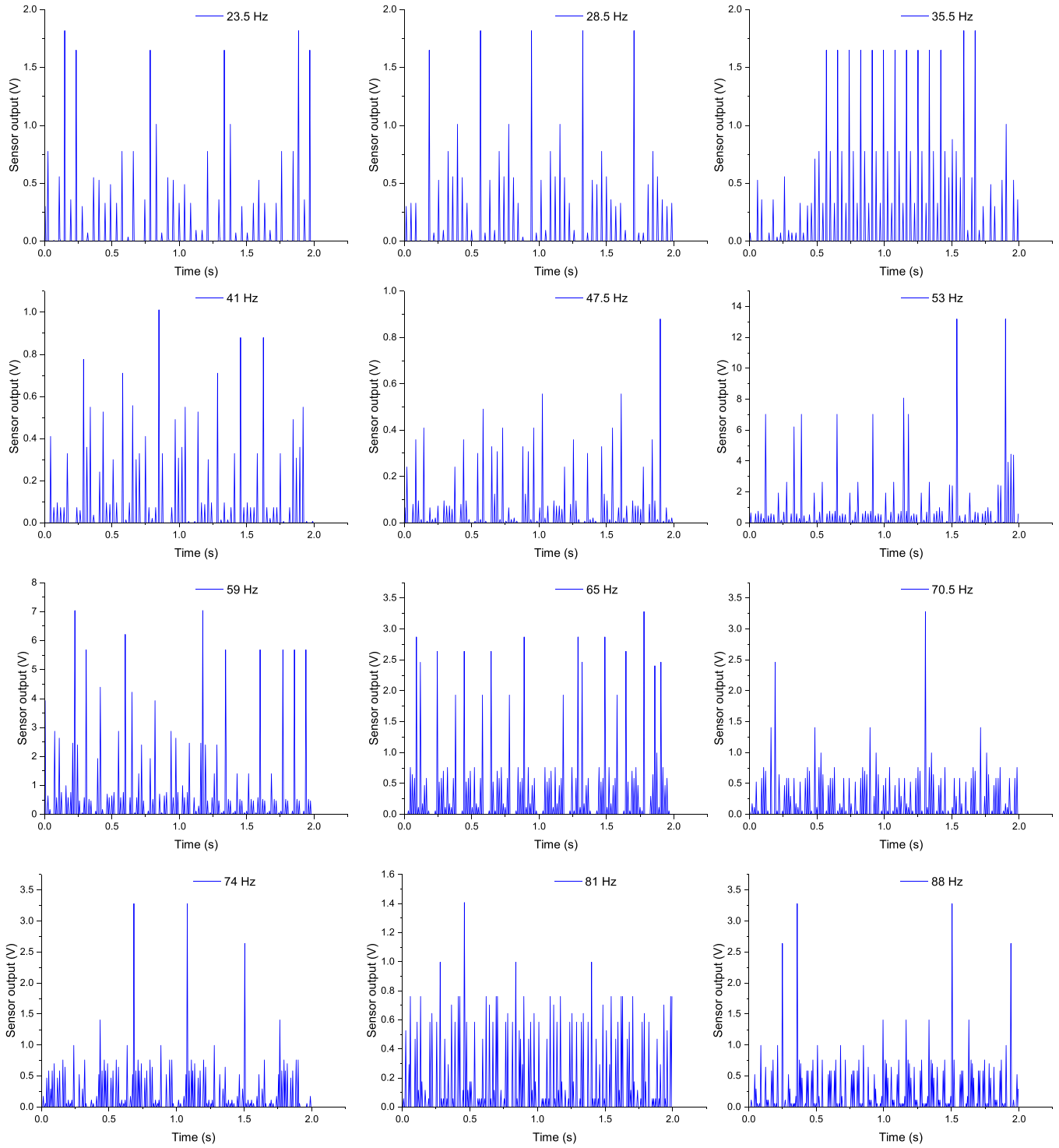

Fig. 4. Amplitude-time graphs of sensor outputs for different frequencies.

$$\widetilde{P}_{xx}^{(i)}(f) = \frac{1}{MU}\left|\sum_{n=0}^{M-1} x_i(n)w(n)e^{-j2\pi fn}\right|^2, i = 0, 1, \ldots, L-1 \quad (2)$$

where M is the length of each segment, L is the number of segments, and U is the normalization factor for the power in the window function, $w(n)$, and is given by Eq. (3).

$$U = \frac{1}{M}\sum_{n=0}^{M-1} w^2(n) \quad (3)$$

The Welch PSD estimation is,

$$P_{xx}^{w}(f) = \frac{1}{L}\sum_{i=0}^{L-1} \widetilde{P}_{xx}^{(i)}(f). \quad (4)$$

The frequency found by the Welch method is equal to the number of rotations of the propeller per second (f_p=rotate per minute/60 s). As given in Eq. (5), the circumference ($2\pi r$) of the propeller is multiplied by its rotation frequency, f_p, to obtain the wind speed, V_w acting on the propeller [53,54].

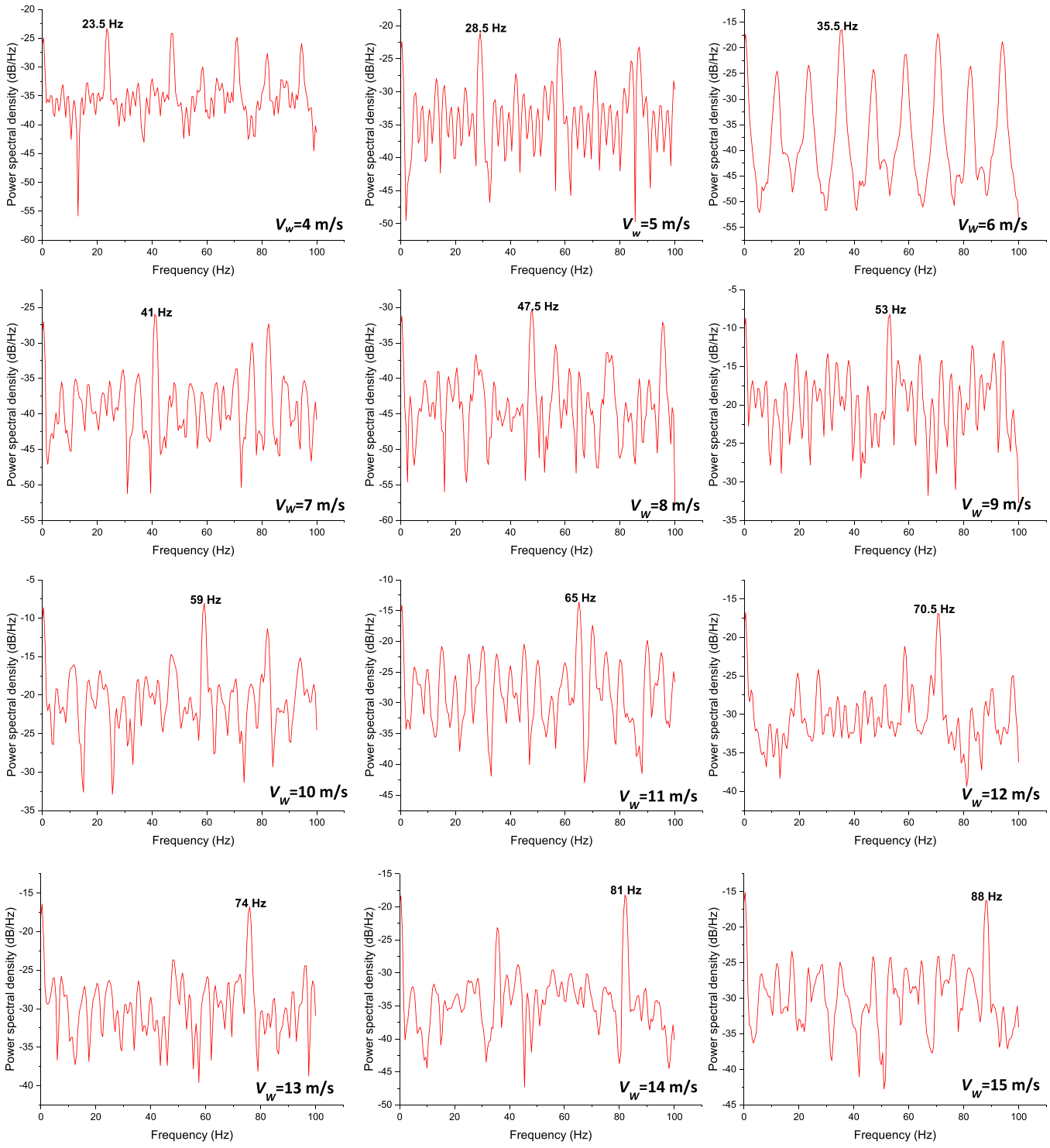

Fig. 5. Propeller frequencies according to different wind speeds.

$$V_w = 2\pi r f_p \tag{5}$$

where the propeller rotation frequency, f_p, is theoretically equal to the maximum amplitude-frequency, f, component of the Welch PSD function.

When the literature is examined, there is a linear equation that includes slope (a) and offset (b) values as in Eq. (6) regarding obtaining the wind speed from the rotating propeller frequency. However, to create this equation, frequency values (f_p) are obtained corresponding to the wind speed applied in a controlled way. Then slope and offset are found by using these frequency values.

$$V_w = af_p + b \tag{6}$$

3. Experimental results and discussion

Wind speeds ranging from 3 m/s to 15 m/s were obtained by adjusting the wind source in a controlled manner with the help of the reference anemometer. Each wind speed was changed in 1 m/s step intervals. The same wind speed also affects the propeller, which is in the

Table 1
Measurement frequencies of the propeller.

V_w (m/s)	$f_{p1\ 11}$ (Hz)	$f_{p2\ 22}$ (Hz)	$f_{p3\ 33}$ (Hz)
3	17	17.5	18
4	23.5	22.5	23.5
5	28.5	29	30
6	35.5	34	34
7	41	40	39
8	47.5	47.5	48
9	53	52	51.5
10	59	58.5	58.5
11	65	65.5	64.5
12	70.5	71	71.5
13	74	73	73.5
14	81	82	80.5
15	88	89	87

same position as the reference anemometer probe. For each fixed wind speed, the analog signal coming to the microcontroller unit is sampled with a sampling period of T = 5 ms, converted into a digital signal, and sent to the computer via the serial port. Therefore, the sampling frequency in the study is f_s= 200 Hz. The signals used in the study consist of 400 samples (2 s). The sampled signal was processed in the MATLAB environment via PC. The Welch PSD of the signals was found using the discrete Fourier transform for 400 points with a segment length of 200 samples and 100 overlapping samples. The time amplitude graph of the received signal against a wind speed of 3 m/s is given in Fig. 3(a). In Fig. 3(b), Welch PSD graph of the signal is given.

Similarly, different wind speeds ranging from 4 m/s to 15 m/s are adjusted in 1 m/s steps, and amplitude-time graphs in 2 s and Welch PSD graphs with 100 Hz bandwidth are shown in Figs. 4 and 5, respectively.

Some amplitude values in Fig. 4 are high (53 Hz, 59 Hz), and some are low (41 Hz, 47.5 Hz). High and low amplitudes are related to the parallelism of the reflective surface and the fiber tip. This change in signal amplitudes does not affect the frequency of the signal.

This whole measurement process was repeated for the second and third times, and the frequencies corresponding to each reference wind speed were obtained by making a total of 39 (3 × 13) separate measurements. The frequencies of the rotating propeller obtained from the measurements are given in Table 1. Here, f_p is the measured frequency values of the propeller rotating at different reference wind speeds. Subscripts represent repeated measurements. As shown in Table 1, the propeller frequency is different for a wind speed measurement because of the change in frictions in the mechanical system to which the propeller is connected. Another reason is the fluctuations in the wind speed of around ± 0.1 m/s. Wind speed is tried to be kept as constant as possible. It has been observed that the propeller frequency at the output of the sensor setup remains constant in long-term measurements as long as the wind speed is kept constant. Accordingly, the wind speed calculated with the help of Eq. (5) remains constant. For this long-term use,

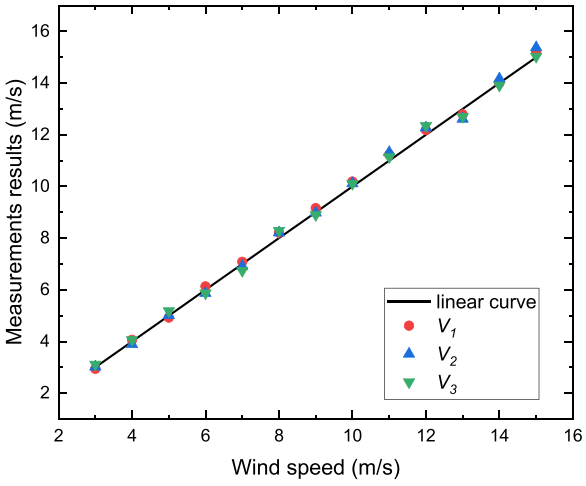

Fig. 6. Repeated measurement results for wind speed measurements of 5.5 cm propeller.

Table 3
Measurement results for the propeller with a diameter of 3 cm.

V_w (m/s)	f (Hz)	V (m/s)	Δ
3	30.5	2.87	-0.13
4	43	4.05	0.05
5	52	4.90	-0.10
6	62	5.84	-0.16
7	72.5	6.83	-0.17
8	85	8.01	0.01
9	97	9.14	0.14
10	109	10.27	0.27
11	120	11.31	0.31
12	124.5	11.73	-0.27
13	136.5	12.86	-0.14
14	147	13.85	-0.15
15	157	14.80	-0.20

after the first two measurement periods, measurements were taken for 30 min for all wind speeds in the third, and it was observed that the wind speeds remained constant.

The diameter of the rotating propeller is 2r = 5.5 cm. Accordingly, the frequencies in Table 1 and the wind speeds calculated using Eq. (5) are given in Table 2. In Table 2, V shows the calculated wind speeds for three different measurements, Δ shows the errors corresponding to each speed measurement and ε_r percentage relative errors. Subscripts represent repeated measurements.

In Table 2, the maximum errors for the first, second, and third measurements are + 0.23 m/s at 11 m/s, − 0.39 m/s at 13 m/s, and + 0.35 m/s at 12 m/s, respectively. In addition, the mean errors in the

Table 2
V, Δ, and ε_r for three measurements.

V_w (m/s)	V_1 (m/s)	V_2 (m/s)	V_3 (m/s)	Δ_1	Δ_2	Δ_3	$\varepsilon_{r1\ 11}$ (%)	$\varepsilon_{r2\ 22}$ (%)	$\varepsilon_{r3\ 33}$ (%)
3	2.94	3.02	3.11	-0.06	0.02	0.11	2.09	0.79	3.67
4	4.06	3.89	4.06	0.06	-0.11	0.06	1.51	2.81	1.51
5	4.92	5.01	5.18	-0.08	0.01	0.18	1.51	0.22	3.67
6	6.13	5.87	5.87	0.13	-0.13	-0.13	2.23	2.09	2.09
7	7.08	6.91	6.74	0.08	-0.09	-0.26	1.20	1.26	3.73
8	8.21	8.21	8.29	0.21	0.21	0.29	2.59	2.59	3.67
9	9.16	8.98	8.90	0.16	-0.02	-0.10	1.75	0.17	1.13
10	10.19	10.11	10.11	0.19	0.11	0.11	1.94	1.08	1.08
11	11.23	11.32	11.14	0.23	0.32	0.14	2.10	2.89	1.32
12	12.18	12.27	12.35	0.18	0.27	0.35	1.51	2.23	2.95
13	12.79	12.61	12.70	-0.21	-0.39	-0.30	1.64	2.97	2.31
14	14.00	14.17	13.91	0.00	0.17	-0.09	0.03	1.20	0.65
15	15.21	15.38	15.03	0.21	0.38	0.03	1.37	2.52	0.22

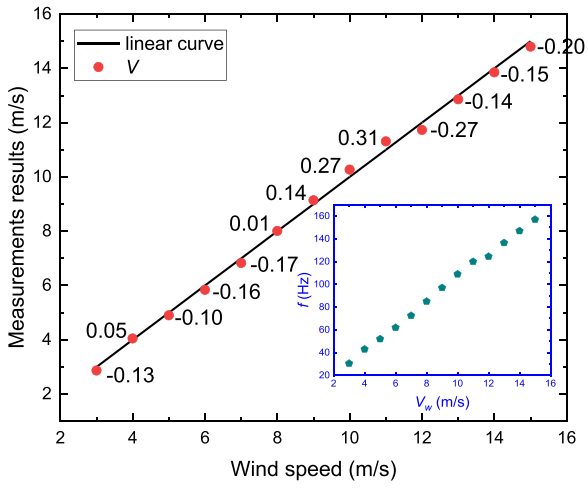

Fig. 7. Measurement results for the propeller with a diameter of 3 cm.

first, second, and third measurements were found to be 0.14, 0.17, and 0.17, respectively. The mean error of all measurements was found to be 0.16. This situation is also shown in Fig. 6 according to linear wind speed variation. The ε_r shown in Table 2 were calculated using Eq. (7).

$$\varepsilon_r = \frac{|V - V_w|}{V_w} \times 100 \tag{7}$$

Where V is the measured speed, and V_w is the reference speed of the wind.

According to the calculations, the maximum ε_r for the first measurement is 2.59% at 8 m/s, the second measurement 2.97% at 13 m/s, and finally 3.73% at 7 m/s for the third measurement. In addition, the mean ε_r in the first, second, and third measurements were found to be 1.65%, 1.76%, and 2.15%, respectively. The average ε_r of all measurements was 1.85%.

In addition to the analyzes made using Eq. (5), Eq. (6) was also evaluated. For this purpose, the wind speed was calculated as $V_W = 0.17129 f_p + 0.02029$ according to the average frequency values with $R^2 = 0.9982$.

The measurement process was repeated to evaluate the effect of propeller size on the measurement, replacing the 5.5 cm diameter propeller in FO-WSMS with another 3 cm diameter propeller. The purpose of this is to show that different propeller sizes do not affect the measured wind speed. For a constant wind speed, the larger diameter propeller has a lower frequency, and the smaller diameter propeller has a higher frequency. This will not cause a change in the measured wind speed. Similar results will be obtained for propellers with different diameters based on Eq. (5). Due to this hardware change, some software changes have also been made. For each wind speed measurement, the signal to the microcontroller was sampled with T = 2.5 ms. Thus, the sampling frequency is $f_s = 400$ Hz. The signals consist of 800 samples. A Welch PSD of the signals was obtained using a segment length of 200 samples and 100 overlapping samples with 800 discrete Fourier transform points. The obtained frequencies, wind speeds, and values of errors are given in Table 3. Eq. (5) has been experimentally verified that the propellers with a lower diameter at constant wind speeds have a higher frequency than those with larger ones.

As shown in Table 3, reasonable errors occur for the 3 cm diameter propeller, like the 5.5 cm diameter propeller results. As shown from Table 3, like the results for the 5.5 cm diameter propeller, reasonable errors also occur for the 3 cm diameter propeller. Fig. 7 is given to show this situation more clearly.

When all these experimental results were examined, lower error values were obtained compared to the closest similar study in the literature. In a similar study, mechanical transmission losses occur due to the presence of mechanical parts, and this increases the error rate [51]. Although there is no mechanical component in our study, the wind is directly applied to the free rotating propeller.

Compared to other methods, the sensor's usability in the wind speed measurement is demonstrated due to its advantages such as technology, cost, ease of manufacturing, EMI interference, ease of measurement, and based on fiber optic. A comparison of the generally used methods was made, as indicated in Table 4.

When the sensor setup is formed by reassembling the units such as the propeller with a reflective surface and the POF coupler, the frequency of the propeller rotating with the effect of the wind can be easily and efficiently re-measured. Different propellers with 3 and 5.5 cm diameters were used in the study, and it was shown that the obtained wind speed was independent of the propeller's diameter. The important point is to know precisely the propeller's diameter used in the setup. It also doesn't matter where the reflective surface is placed on the propeller. The reflective surface and the coupler tip must be aligned. When these simple conditions are met, different sensor setups can operate at the same performance.

4. Conclusion

In this article, an optomechanical fiber anemometer based on Fresnel reflection is designed and realized. Depending on the effective wind speed, the rotating propeller's frequency is measured with high accuracy by a rotate per minute detection system. This measurement process is based on the return of the light hitting the reflector on the propeller surface to a fiber optic card with the help of an optical coupler, then converting it into an electrical signal and transferring it to the microcontroller chip (ATmega328P) and converting it into a digital signal by processing in this chip. Then, the frequency of the digital signal is obtained via a PC, and the wind speed is determined. When the multiple measurement results are evaluated, the highest error value is 0.39 m/s, and the highest percent relative error value is 3.73%. The mean error value for all measurements was 0.16, and the mean percentage relative error value was 1.85%. In addition, experiments were carried out for propellers of different diameters to evaluate the propeller diameter effect. The results show that the proposed FO-WSMS is successful in wind speed measurement. This system provides convenience to users in challenging environmental conditions as it has the advantages of fiber optics such as electromagnetic immunity, lightness, and low cost.

Table 4
Comparison of literature.

Technology	Cost	Ease of manufacturing	EMI interference	Ease of measurement	Based on fiber optic	References
Mechanical	Medium	Medium	High	High	No	[9]
Hot wire	Medium	Low	High	High	No	[10]
Ultrasonic	High	Low	High	High	No	[11]
Lidar	High	Low	High	High	No	[12]
FBG based	High	Low	Low	Medium	Yes	[25–39]
Fabry-P é rot interferometer	High	Low	Low	Medium	Yes	[41]
SMS-MMI reflective bend	High	Low	Low	Medium	Yes	[42]
Fiber optic curvature sensor	Medium	Low	Low	High	Yes	[51]
Fresnel reflection	Low	High	Low	High	Yes	This study

Declaration of Competing Interest

The authors declare that they have no known competing financial interests or personal relationships that could have appeared to influence the work reported in this paper.

References

[1] D.Y. Leung, Y. Yang, Wind energy development and its environmental impact: a review, Renew. Sustain. Energy Rev. 16 (1) (2012) 1031–1039.
[2] C. Emeksiz, T. Cetin, In case study: Investigation of tower shadow disturbance and wind shear variations effects on energy production, wind speed and power characteristics, Sustain. Energy Technol. Assess. 35 (2019) 148–159.
[3] J. Li, X. Yu, Model and procedures for reliable near term wind energy production forecast, Wind Eng. 39 (6) (2015) 595–607.
[4] P. Tavner, C. Edwards, A. Brinkman, F. Spinato, Influence of wind speed on wind turbine reliability, Wind Eng. 30 (1) (2006) 55–72.
[5] M.Z. Jacobson, M.Z. Jacobson, Fundamentals of Atmospheric Modeling, Cambridge university press, 2005.
[6] S. Rehman, M.A. Mohandes, L.M. Alhems, Wind speed and power characteristics using LiDAR anemometer-based measurements, Sustain. Energy Technol. Assess. 27 (2018) 46–62.
[7] M.A. Mohamed, A.M. Eltamaly, A.I. Alolah, PSO-based smart grid application for sizing and optimization of hybrid renewable energy systems, PloS One 11 (8) (2016), e0159702.
[8] T.A. Burdett, K.W. Van Treuren, Small-Scale Wind Turbines Optimized for Class 2 Wind: A Wind Siting Survey and Annual Energy Production Analysis, in: Turbo Expo: Power for Land, Sea, and Air, 45660, American Society of Mechanical Engineers, 2014.
[9] Gutarra, J.S., Gastelo-Roque, J.A., & Sulluchuco, J. (2020, September). A cup anemometer using 3D additive manufacturing. In 2020 IEEE XXVII International Conference on Electronics, Electrical Engineering and Computing (INTERCON) (pp. 1–4). IEEE.
[10] F. Daniel, J. Peyrefitte, A.D. Radadia, Towards a completely 3D printed hot wire anemometer, Sens. Actuators A Phys. 309 (2020), 111963.
[11] del Valle, M.P., Castelan, J.A. U., Matsumoto, Y., & Mateos, R.C. (2007, September). Low cost ultrasonic anemometer. In 2007 4th International Conference on Electrical and Electronics Engineering (pp. 213–216). IEEE.
[12] Hardesty, R.M., & Intrieri, J.M. (1995, April). Doppler lidar measurements of wind and turbulence in the marine boundary layer. In Conference Proceedings Second Topical Symposium on Combined Optical-Microwave Earth and Atmosphere Sensing (pp. 148–150). IEEE.
[13] C.Y. Huang, P.W. Chan, H.Y. Chang, W.F. Liu, A fiber bragg grating-based anemometer, Sensors 18 (7) (2018) 2213.
[14] Á. Ramos-Cenzano, E. López-Núñez, D. Alfonso-Corcuera, M. Ogueta-Gutiérrez, S. Pindado, On cup anemometer performance at high altitude above ground, Flow. Meas. Instrum. 79 (2021), 101956.
[15] Y. Bai, X. Meng, H. Guo, D. Liu, Y. Jia, P. Cui, Design and validation of an adaptive low-power detection algorithm for three-cup anemometer, Measurement 172 (2021), 108887.
[16] G. Zhang, J.S. Strøm, P. Ravn, E.F. Kristensen, Performance testing of a large, free-blowing propeller and a method for measuring flow rate, Biosyst. Eng. 110 (4) (2011) 458–464.
[17] R. Joseph, Air flow analysis with a vane anemometer, Met. Finish. 102 (5) (2004) 50–52.
[18] P. Ligęza, An alternative mathematical model of vane anemometers based on the balance of power, Flow. Meas. Instrum. 54 (2017) 210–215.
[19] C. Cui, W. Cai, H. Chen, Airflow measurements using averaging Pitot tube under restricted conditions, Build. Environ. 139 (2018) 17–26.
[20] Ogueta-Gutiérrez, M., & Pindado, S. Performance analysis of present cup anemometers. Journal of Energy Systems, 3(4), 129–138.
[21] A. Ramos-Cenzano, M. Ogueta-Gutiérrez, S. Pindado, Cup anemometer measurement errors due to problems in the output signal generator system, Flow. Meas. Instrum. 69 (2019), 101621.
[22] M. Parrilla, J.J. Anaya, C. Fritsch, Digital signal processing techniques for high accuracy ultrasonic range measurements, IEEE Trans. Instrum. Meas. 40 (4) (1991) 759–763.
[23] S.F. Benjamin, C.A. Roberts, Measuring flow velocity at elevated temperature with a hot wire anemometer calibrated in cold flow, Int. J. Heat Mass Transf. 45 (4) (2002) 703–706.
[24] D.J. Tritton, The use of a fibre anemometer in turbulent flows, J. Fluid Mech. 16 (2) (1963) 269–281.
[25] Y. Zhang, F. Wang, Z. Duan, Z. Liu, Z. Liu, Z. Wu, W. Peng, A novel low-power-consumption all-fiber-optic anemometer with simple system design, Sensors 17 (9) (2017) 2107.
[26] Y. Zhang, F. Wang, Z. Liu, Z. Duan, W. Cui, J. Han, W. Peng, Fiber-optic anemometer based on single-walled carbon nanotube coated tilted fiber Bragg grating, Opt. Express 25 (20) (2017) 24521–24530.
[27] J.N. Cheng, H.Y. Chang, M.Y. Fu, W.F. Liu, Fiber anemometer for simultaneously measuring wind speed and wind direction, Microw. Opt. Technol. Lett. 61 (4) (2019) 891–896.
[28] Wang, F., Zhang, Y., Duan, Z., Jing, Z., Zhou, D., & Peng, W. (2018, October). Fiber-optic anemometer with intensity linear demodulation. In 2018 Asia Communications and Photonics Conference (ACP) (pp. 1–3). IEEE.
[29] Huang, C.Y., Chan, P.W., Chang, H.Y., & Liu, W.F. (2018, April). The fiber anemometer based on fiber gratings. In 2018 IEEE International Conference on Applied System Invention (ICASI) (pp. 1012–1014). IEEE.
[30] Lai, Y.Y., Ho, Y.S., & Liang, T.C. (2019, April). Design a Wind Speed and Direction Sensor Based on Fiber Bragg Grating. In 2019 IEEE International Conference of Intelligent Applied Systems on Engineering (ICIASE) (pp. 59–61). IEEE.
[31] Z. Liu, F. Wang, Y. Zhang, Z. Jing, W. Peng, Low-power-consumption fiber-optic anemometer based on long-period grating with SWCNT coating, IEEE Sens. J. 19 (7) (2019) 2592–2597.
[32] Y. Liu, B. Liang, X. Zhang, N. Hu, K. Li, F. Chiavaioli, T. Guo, Plasmonic fiber-optic photothermal anemometers with carbon nanotube coatings, J. Light. Technol. 37 (13) (2019) 3373–3380.
[33] F. Wang, Y. Duan, M. Lu, Y. Zhang, Z. Jing, C. Sun, W. Peng, Fiber-optic hot-wire anemometer with directional response based on symmetry-breaking induced heat transfer mechanism, J. Light. Technol. 39 (12) (2021) 3919–3925.
[34] Yang, J., Chen, X., & Dong, X. (2020). Hot-wire anemometer based on frosted fiber Bragg grating coated with silver film. In IOP Conference Series: Materials Science and Engineering (Vol. 711, No. 1, p. 012112). IOP Publishing.
[35] S. Gao, A.P. Zhang, H.Y. Tam, L.H. Cho, C. Lu, All-optical fiber anemometer based on laser heated fiber Bragg gratings, Opt. Express 19 (11) (2011) 10124–10130.
[36] Y. Liu, W. Peng, X. Zhang, Y. Liang, Z. Gong, M. Han, Fiber-optic anemometer based on distributed Bragg reflector fiber laser technology, IEEE Photonics Technol. Lett. 25 (13) (2013) 1246–1249.
[37] X. Wang, X. Dong, Y. Zhou, K. Ni, J. Cheng, Z. Chen, Hot-wire anemometer based on silver-coated fiber Bragg grating assisted by no-core fiber, IEEE Photonics Technol. Lett. 25 (24) (2013) 2458–2461.
[38] X. Wang, X. Dong, Y. Zhou, Y. Li, J. Cheng, Z. Chen, Optical fiber anemometer using silver-coated fiber Bragg grating and bitaper, Sens. Actuators A: Phys. 214 (2014) 230–233.
[39] J. Wang, Z.Y. Liu, S. Gao, A.P. Zhang, Y.H. Shen, H.Y. Tam, Fiber-optic anemometer based on Bragg grating inscribed in metal-filled microstructured optical fiber, J. Light. Technol. 34 (21) (2016) 4884–4889.
[40] R. Díaz, C.A. Leal-Junior, A.G. Avellar M., L. Antunes C., P.F. Pontes, M.J. Marques, C. A, M.R. N Ribeiro, Perrogator: a portable energy-efficient interrogator for dynamic monitoring of wavelength-based sensors in wearable applications, Sensors 19 (13) (2019) 2962.
[41] G. Liu, W. Hou, W. Qiao, M. Han, Fast-response fiber-optic anemometer with temperature self-compensation, Opt. Express 23 (10) (2015) 13562–13570.
[42] J.W. Costa, M.A. Franco, V.A. Serrão, C.M. Cordeiro, M.T. Giraldi, Macrobending SMS fiber-optic anemometer and flow sensor, Opt. Fiber Technol. 52 (2019), 101981.
[43] A.G. Leal-Junior, A. Frizera, C. Marques, M.R. Sanchez, T.R. Botelho, M.V. Segatto, M.J. Pontes, Polymer optical fiber strain gauge for human-robot interaction forces assessment on an active knee orthosis, Opt. Fiber Technol. 41 (2018) 205–211.
[44] A. Leal-Junior, A. Frizera, C. Díaz, C. Marques, M. Ribeiro, M.J. Pontes, Material features based compensation technique for the temperature effects in a polymer diaphragm-based FBG pressure sensor, Opt. Express 26 (16) (2018) 20590–20602.
[45] Y. Wang, Y. Huang, H. Bai, G. Wang, X. Hu, S. Kumar, R. Min, Biocompatible and biodegradable polymer optical fiber for biomedical application: a review, Biosensors 11 (12) (2021) 472.
[46] C. Leitão, A. Leal-Junior, A.R. Almeida, S.O. Pereira, F.M. Costa, J.L. Pinto, C. Marques, Cortisol AuPd plasmonic unclad POF biosensor, Biotechnol. Rep. 29 (2021), e00587.
[47] T.E. Tabaru, The temperature effect on U and coil shaped POF sensors to detect refractive index change, Fiber Integr. Opt. 40 (1) (2021) 48–69.
[48] Ş.E. Hayber, T.E. Tabaru, M. Güçyetmez, Evanescent field absorption-based fiber optic sensor for detecting power transformer oil degradation, Fiber Integr. Opt. (2021) 1–20.
[49] Plastic Optical Fiber, in: M.M. Werneck, R.C.S. Allil (Eds.), Sensors: Science, Technology and Applications, CRC Press, 2019.
[50] J. Zubia, O. Aresti, J. Arrúe, M. Lopez-Amo, Barrier sensor based on plastic optical fiber to determine the wind speed at a wind generator, IEEE J. Sel. Top. Quantum Electron. 6 (5) (2000) 773–779.
[51] G. Zhi, H. Di, Wind speed monitoring system based on optical fiber curvature sensor, Opt. Fiber Technol. 62 (2021), 102467.
[52] J.G. Proakis, D.G. ve Manolakis, Digital Signal Processing Principles, Algorithms, and Applications, Prentice-Hall, New Jersey, 1996.
[53] Reddy, G.K. K., Reddy, S.V., & Ramkumar, T.K. (2012, December). Development of Hall sensor propeller anemometer for measuring wind speed using embedded controller. In 2012 International Conference on Communications, Devices and Intelligent Systems (CODIS) (pp. 484–487). IEEE.
[54] Babu, S.D., Acharjya, A.S., & Alam, S. (2014, October). Design & construction of microcontroller based wind speed & direction monitoring system. In 2014 9th International Forum on Strategic Technology (IFOST) (pp. 284–288). IEEE.

Mehmet Güçyetmez received his B.Sc. and M.Sc. degrees from Erciyes University Electrical and Electronics Engineering Department in 2003 and 2005, respectively. He received his Ph.D. degree from Kırıkkale University Electrical and Electronics Engineering Department in 2016. He is currently working as an Assistant Professor in the Department of Electrical and Electronics Engineering at Kırşehir Ahi Evran University. His interest areas are electric transmission and distribution, renewable energy sources, power system analysis, power system control and optimization and instrumentation in power systems.

Serkan Keser received the M.S. and Ph.D. degrees from Eskişehir Osmangazi University, both in Electrical-Electronics Engineering, in 2008 and 2018, respectively. He is working as an Asst. Prof. at the Department of Electrical and Electronics Engineering, Kırşehir Ahi Evran University. His current research interests are signal and systems, digital signal processing, speech and image recognition, signal coding and artificial neural networks.

Şekip Esat Hayber received the M.S. and Ph.D. degrees in the Department of Electrical-Electronics Engineering from Erciyes University, Kayseri, Turkey, in 2011 and 2018, respectively. He is currently working as an Assistant Professor in the Department of Electrical and Electronics Engineering at Kırşehir Ahi Evran University. His research involves optic and fiber optic detection, optical fiber sensing system, photonic sensors.